

An Adaptive Multivariate Functional EWMA Control Chart

Christian Capezza¹, Giovanna Capizzi², Fabio Centofanti¹, Antonio Lepore^{1*}, and Biagio Palumbo¹

¹*Department of Industrial Engineering, University of Naples Federico II, Piazzale Tecchio 80, 80125, Napoli, Italy*

²*Department of Statistical Sciences, University of Padua, Via Cesare Battisti 241, 35121, Padova, Italy*

* *Corresponding author: antonio.lepore@unina.it*

Abstract

In many modern industrial scenarios, the measurements of the quality characteristics of interest are often required to be represented as functional data or profiles. This motivates the growing interest in extending traditional univariate statistical process monitoring (SPM) schemes to the functional data setting. This article proposes a new SPM scheme, which is referred to as adaptive multivariate functional EWMA (AMFEWMA), to extend the well-known exponentially weighted moving average (EWMA) control chart from the univariate scalar to the multivariate functional setting. The favorable performance of the AMFEWMA control chart over existing methods is assessed via an extensive Monte Carlo simulation. Its practical applicability is demonstrated through a case study in the monitoring of the quality of a resistance spot welding process in the automotive industry through the online observations of dynamic resistance curves, which are associated with multiple spot welds on the same car body and recognized as the full technological signature of the process.

Keywords: Functional Data Analysis, Profile Monitoring, Statistical Process Control

1 Introduction

The main aim of statistical process monitoring (SPM) is to detect special causes of variation possibly acting on a process, which is then said to be out of control (OC). Otherwise, it is said to be in control (IC). As is known, SPM is currently implemented in two phases. The first one (Phase I) is concerned with identifying a clean data set to be assumed as representative of the IC state of the process, named Phase I sample, while the second one (Phase II) aims at the prospective monitoring of new observations (Qiu, 2014), often referred to as Phase II observations or data set.

In modern industrial SPM, the capability of new data acquisition systems is reshaping the size and the variety of signals and measurements available, which are often functions of time or space and can be best characterized by functional variables or profiles (Ramsay and Silverman, 2005; Kokoszka and Reimherr, 2017). The simplest approach for the monitoring of one or multiple quality characteristics in this form is the application of classical SPM techniques for multivariate data (Montgomery, 2019) on scalar features extracted from them, although this simple approach risks being problem-specific, arbitrary, and flattening useful information.

To avoid that, profile monitoring (Noorossana et al., 2011) aims to directly monitor quality characteristics in the form of one or multiple functional variables. Some recent examples are those of Jin and Shi (1999); Colosimo and Pacella (2010); Zou et al. (2012); Chou et al. (2014); Grasso et al. (2014); Paynabar et al. (2016); Grasso et al. (2016, 2017); Menafoglio et al. (2018); Maleki et al. (2018); Wang et al. (2018); Ren et al. (2019); Jones et al. (2021); Centofanti et al. (2021); Capezza et al. (2022a,b). These contributions are based on functional extensions of the Shewart control chart and allow the process state to be assessed only on the information acquired at the current point in time, without considering previous data points, which may contain decisive information about process condition trends. For this reason, the Shewart control chart may be particularly ineffective in detecting small persistent shifts.

The exponentially weighted moving average (EWMA) control chart is instead known to overcome this limitation by evaluating the current state of the process through a statistic calculated as a weighted average of the observation at the current point in time and the

statistic itself at the previous point. The weighted average is determined by a single weighting parameter, usually denoted with λ (Qiu, 2014), such that $0 \leq \lambda \leq 1$. Although the design, implementation, and properties of the EWMA control chart have been widely discussed for both univariate and multivariate quality characteristics (Crowder, 1989; Gan, 1993; Serel, 2009; Chan and Zhang, 2000; Lucas and Saccucci, 1990; Capizzi and Masarotto, 2003; Knoth, 2007; Lowry et al., 1992; Jones et al., 2001), few extensions have been proposed in the profile monitoring literature in this regard. It is worth mentioning Fassò et al. (2016), who developed a functional EWMA control chart for both univariate and multivariate functional data. In particular, they applied a multivariate EWMA control chart to the basis coefficients resulting from a chosen finite-dimensional representation of the functional data in the reference sample. Ren et al. (2019) move forward with the integration of the EWMA scheme with the multichannel functional principal component analysis, developed by Paynabar et al. (2016) for the Phase II monitoring of multichannel profiles.

The major challenge for any EWMA control chart is related to the choice of the weighting parameter λ , which should minimize the average run length (ARL) defined as the average number of observations required to signal an OC state with respect to a specified shift (Lucas and Saccucci, 1990). The ARL corresponding to no shift is usually referred to as IC ARL. It is known that the smaller the value of λ , the smaller the shift with respect to which the ARL is the minimum for a given IC ARL. However, in most real cases, there is no prior information available on the magnitude of the shift that may actually occur in the OC scenario.

Therefore, methods are needed for adaptively selecting λ such that the resulting EWMA control chart performs adequately in a wide range of OC conditions. In the univariate scalar setting, this issue is addressed by the adaptive EWMA (AEWMA) control chart proposed by Capizzi and Masarotto (2003) that smoothly combines EWMA and Shewhart control charting schemes, by adaptively selecting the weighting parameter through a suitable function of the magnitude of the difference between the current observation and the monitoring statistic observed up to the previous point in time. This idea has been extended to the multivariate setting (Mahmoud and Zahran, 2010; Haq and Khoo, 2019), but has never been addressed in the profile monitoring literature.

In this work, we propose a new method for the monitoring of a process through observations of a multivariate functional quality characteristic, which is named adaptive multivariate functional EWMA (AMFEWMA) control chart and extends the underlying idea of Capizzi and Masarotto (2003) to the multivariate profile monitoring setting. As a case study, we consider the monitoring of a resistance spot welding (RSW) process in the automotive body-in-white manufacturing (Zhang and Senkara, 2011). RSW is commonly used to join overlapping steel galvanized sheets by means of two copper electrodes to guarantee the structural integrity and solidity of welded assemblies in each vehicle (Martín et al., 2014). In this context, the dynamic resistance curve (DRC) is considered as highly representative of the physical and metallurgical development of a spot weld (Capezza et al., 2021), and therefore, of the quality of the joint produced. In particular, there is a consensus among experts regarding the correlation between the latter and the degradation status or wear level of the electrodes (Manladan et al., 2017). A control chart capable of accommodating varying degrees of mean shift, contingent upon different wear levels, without prior knowledge about the current wear level, can prove immensely advantageous.

The paper is structured as follows. Section 2 introduces the AMFEWMA control chart. Section 3 reports a Monte Carlo simulation study of the performance of the AMFEWMA control chart in identifying process mean shifts of a multivariate functional quality characteristic with respect to other non-adaptive SPM approaches that have already been presented in the literature. The practical applicability of the proposed method is demonstrated in Section 4 through a case study in the SPM of multivariate DRCs from a RSW process in automotive body-in-white manufacturing. Section 5 concludes the paper. Supplementary Materials that provide details on data generation in the simulation study are available online. All computations and plots have been obtained using the R programming language (R Core Team, 2023).

2 The AMFEWMA control chart

The elements of the AMFEWMA control chart are developed in the following sections. Section 2.1 shows how smooth functional data are obtained from the original discrete observations for each curve; Section 2.2 illustrates the multivariate functional principal

component analysis (MFPCA); Section 2.3 introduces the AMFEWMA scheme, while its design and implementation details are referred to Section 2.4.

2.1 Data Smoothing

For each profile, measurements y_i , $i = 1, \dots, m$, of the quality characteristic are supposed to be collected in a discrete fashion with the observation points $t_1, \dots, t_m \in \mathcal{T} \subset \mathbb{R}$, into a realization X of a random function with values in $L^2(\mathcal{T})$, i.e., the Hilbert space of square integrable functions defined on the compact set $\mathcal{T} \subset \mathbb{R}$, with inner product between $a, b \in L^2(\mathcal{T})$ given by $\langle a, b \rangle = \int_{\mathcal{T}} a(t)b(t)dt$. Hence, methods are required to convert discrete raw data $\{(t_i, y_i)\}_{i=1, \dots, m}$ into functional data X . If the discrete data are assumed without any measurement error, functional data can be theoretically drawn up by merely connecting the whole set of points $\{(t_i, y_i)\}$. However, this does not represent the ordinary situation. When measurement error is present, each discrete observation is expressed as

$$y_i = X(t_i) + \varepsilon_i, \quad i = 1, \dots, m, \quad (1)$$

for $i = 1, \dots, m$, where ε_i are independent identically distributed random errors with zero mean. The functional variable X is intrinsically infinite dimensional, that is infinite features would be needed to completely specify it at each possible argument $t \in \mathcal{T}$. Therefore, from Equation (1), data smoothing techniques are commonly used to recover X by discarding exogenous perturbation due to error terms ε_i . A common approach consists of representing X through a linear combination of K known basis functions $\boldsymbol{\phi} = (\phi_1, \dots, \phi_K)^T$. That is,

$$X(t) = \sum_{k=1}^K c_k \phi_k(t) = \mathbf{c}^T \boldsymbol{\phi}(t) \quad t \in \mathcal{T}, \quad (2)$$

where $\mathbf{c} = (c_1, \dots, c_K)^T$ is the vector of basis coefficients. The value of K is not crucial unless it is sufficiently large to capture the local behavior of the functional data (Cardot et al., 2003). Then, the problem of recovering X from the discrete raw data reduces to finding the estimate $\hat{\mathbf{c}}$ of the unknown coefficient vector \mathbf{c} , which is obtained by minimizing

the following penalized sum of squares error

$$\hat{\mathbf{c}} = \operatorname{argmin}_{\mathbf{c} \in \mathbb{R}^K} \sum_{i=1}^m (y_i - \mathbf{c}^T \boldsymbol{\phi}(t_i))^2 + \lambda_s \mathbf{c}^T \mathbf{R} \mathbf{c}, \quad (3)$$

where $\lambda_s > 0$ is a smoothing parameter and \mathbf{R} is a matrix whose entries are $\langle \phi_i^{(d)}(t), \phi_j^{(d)} \rangle$, with $\phi^{(d)}$ denoting the d -th derivative of ϕ . The smoothing parameter λ_s is chosen by minimizing the generalized cross-validation (GCV) criterion, which is a well-known method to achieve a trade-off between variance and bias. This criterion takes into account the degrees of freedom of the estimated curve that vary according to λ_s . The reader may want to refer to Ramsay and Silverman (2005) for further details. The matrix \mathbf{R} , which controls the penalty on the right-hand side of Equation (3), is usually computed by setting $d = 2$, i.e., by penalizing the function roughness.

The functional datum $\hat{X}(t)$ so estimated is

$$\hat{X}(t) = \hat{\mathbf{c}}^T \boldsymbol{\phi}(t) \quad t \in \mathcal{T}. \quad (4)$$

The most common choice for $\boldsymbol{\phi}$ in case of non-periodic functional data is the B-spline basis system, owing good computational properties and great flexibility (Ramsay and Silverman, 2005). More in general, splines are known to be optimal in the sense of being the smoothest functions interpolating the data (Green and Silverman, 1993). Spline functions divide the functional domain into subintervals, by means of breakpoints. Over any subinterval, the spline is a polynomial of order q , with $q - 1$ non-zero derivatives and matching proper derivative constraints between adjacent polynomials (De Boor, 1978).

2.2 Multivariate Functional Principal Component Analysis

Let us consider a random vector $\mathbf{X} = (X_1, \dots, X_p)^T$ with realizations in \mathbb{H} , the Hilbert space of p -dimensional vectors of functions in $L^2(\mathcal{T})$. Given two elements $\mathbf{a}, \mathbf{b} \in \mathbb{H}$, where $\mathbf{a} = (a_1, \dots, a_p)^T$ and $\mathbf{b} = (b_1, \dots, b_p)^T$, the inner product of \mathbb{H} is defined as $\langle \mathbf{a}, \mathbf{b} \rangle_{\mathbb{H}} = \sum_{j=1}^p \langle a_j, b_j \rangle$. We assume that \mathbf{X} has mean $\boldsymbol{\mu} = (\mu_1, \dots, \mu_p)^T$, where $\mu_j(t) = \mathbb{E}(X_j(t))$, $j = 1, \dots, p$, $t \in \mathcal{T}$ and covariance $\mathbf{C} = \{C_{jk}\}_{1 \leq j, k \leq p}$, $C_{jk}(s, t) = \operatorname{Cov}(X_j(s), X_k(t))$,

$s, t \in \mathcal{T}$. From the multivariate Karhunen-Loève's Theorem (Happ and Greven, 2018) it follows that

$$\mathbf{X}(t) - \boldsymbol{\mu}(t) = \sum_{l=1}^{\infty} \xi_l \boldsymbol{\psi}_l(t), \quad t \in \mathcal{T},$$

where $\xi_l = \langle \boldsymbol{\psi}_l, \mathbf{Z} \rangle_{\mathbb{H}}$ are random variables, say *principal components scores* or simply *scores*, such that $E(\xi_l) = 0$ and $E(\xi_l \xi_m) = \rho_l \delta_{lm}$, with δ_{lm} denoting the Kronecker delta. The elements of the orthonormal set $\{\boldsymbol{\psi}_l\}_{l \geq 1}$, $\boldsymbol{\psi}_l = (\psi_{l1}, \dots, \psi_{lp})^T$, with $\langle \boldsymbol{\psi}_l, \boldsymbol{\psi}_m \rangle_{\mathbb{H}} = \delta_{lm}$, are referred to as *principal components*, and are the eigenfunctions of the covariance \mathbf{C} of \mathbf{Z} corresponding to the eigenvalues $\rho_1 \geq \rho_2 \geq \dots \geq 0$.

MFPCA aims to estimate $\boldsymbol{\psi}_l$ and ρ_l , $l \geq 1$, starting from N independent realizations, $\mathbf{X}_1, \dots, \mathbf{X}_N$, of \mathbf{X} , where $\mathbf{X}_i = (X_{i1}, \dots, X_{ip})^T$, which can be obtained through the data smoothing technique described in Section 2.1 and denoted by $\hat{\mathbf{X}}_1, \dots, \hat{\mathbf{X}}_N$. That is, each X_{ij} , $j = 1, \dots, p$, is estimated as $\hat{X}_{ij}(t) = \hat{\mathbf{c}}_{ij}^T \boldsymbol{\phi}(t)$, where $\hat{\mathbf{c}}_{ij} = (\hat{c}_{ij1}, \dots, \hat{c}_{ijK})^T$. Following the basis function expansion approach of Ramsay and Silverman (2005), each component ψ_{lj} of $\boldsymbol{\psi}_l$ is represented as the following linear combination of the K basis functions ϕ_1, \dots, ϕ_K used to obtain $\hat{\mathbf{X}}_1, \dots, \hat{\mathbf{X}}_N$

$$\psi_{lj}(t) = \sum_{k=1}^K b_{ljk} \phi_k(t), \quad t \in \mathcal{T}, \quad j = 1, \dots, p, \quad l = 1, 2, \dots, \quad (5)$$

where $\mathbf{b}_{lj} = (b_{lj1}, \dots, b_{ljK})^T$ are the eigenfunction coefficient vectors. Under these assumptions, MFPCA (Ramsay and Silverman, 2005; Chiou et al., 2014) consists of performing standard multivariate principal component analysis of the random vectors $\mathbf{W}^{1/2}(\hat{\mathbf{c}}_i - \bar{\mathbf{c}})$, where $\hat{\mathbf{c}}_i = (\hat{\mathbf{c}}_{i1}^T, \dots, \hat{\mathbf{c}}_{ip}^T)^T$, $\bar{\mathbf{c}} = \sum_{i=1}^N \hat{\mathbf{c}}_i / N$ and \mathbf{W} is a block-diagonal matrix with diagonal blocks \mathbf{W}_j , $j = 1, \dots, p$, whose entries are $w_{k_1 k_2} = \langle \phi_{k_1}, \phi_{k_2} \rangle$, $k_1, k_2 = 1, \dots, K$. Specifically, the estimated eigenvalues $\hat{\rho}_l$ of \mathbf{C} are the eigenvalues of the sample covariance matrix \mathbf{S} obtained from $\mathbf{W}^{1/2}(\hat{\mathbf{c}}_i - \bar{\mathbf{c}})$, whereas $\hat{\boldsymbol{\psi}}_l = (\hat{\psi}_{l1}, \dots, \hat{\psi}_{lp})^T$ is obtained through Equation (5), where $\mathbf{b}_{lj} = \mathbf{W}^{-1/2} \mathbf{u}_{lj}$ and $\mathbf{u}_l = (\mathbf{u}_{l1}^T, \dots, \mathbf{u}_{lp}^T)^T$ is the l -th eigenvector of \mathbf{S} .

In practice, it is assumed that, as the eigenvalues decrease toward zero, the leading eigenfunctions tend to reflect the most important features of \mathbf{X} . That is, $\hat{\mathbf{X}}_i$ are approxi-

mated by $\hat{\mathbf{X}}_i^L$ through the following truncated principal component decomposition

$$\hat{\mathbf{X}}_i^L(t) = \hat{\boldsymbol{\mu}}(t) + \hat{\mathbf{D}}(t) \sum_{l=1}^L \hat{\xi}_{il} \hat{\boldsymbol{\psi}}_l(t) \quad t \in \mathcal{T}, \quad (6)$$

where $\hat{\mathbf{D}}$ is a $p \times p$ diagonal matrix whose diagonal entries are $\hat{v}_j^{1/2}$ and $\hat{\xi}_{il} = \langle \hat{\boldsymbol{\psi}}_l, \hat{\mathbf{X}}_i \rangle_{\mathbb{H}}$. In the profile monitoring literature, the parameter L is generally chosen such that the retained principal components explain at least a given percentage of the total variability, which is usually in the range 70-90% (Paynabar et al., 2016; Ren et al., 2019; Centofanti et al., 2022; Capezza et al., 2022b), even though more sophisticated methods can be used as well (Jolliffe and Cadima, 2016; Capezza et al., 2020).

2.3 The monitoring scheme

Let us consider a sequence of independent realizations in \mathbb{H} of the random vector $\mathbf{X}_n = (X_{n1}, \dots, X_{np})^T$, $n = 1, 2, \dots$. Suppose that (a) before an unknown observation, say n_0 , the process is in control and the mean is equal to a target value $\boldsymbol{\mu}_0$, (b) after n_0 , the mean becomes $\boldsymbol{\mu}_1 = \boldsymbol{\mu}_0 + \boldsymbol{\delta}$, where $\boldsymbol{\delta}$ is an unknown shift, and (c) we want to detect the occurrence of this shift as soon as possible. Without loss of generality, it is assumed that, when the process is in control, the data are mean centered, i.e., $\boldsymbol{\mu}_0$ is a vector of zero functions. As in Fassò et al. (2016), an EWMA control chart for multivariate functional data can be built based on the statistic $\tilde{\mathbf{Y}}_n = (\tilde{Y}_{n1}, \dots, \tilde{Y}_{np})^T$, defined as

$$\tilde{\mathbf{Y}}_n(t) = (\mathbf{I} - \boldsymbol{\Lambda})\tilde{\mathbf{Y}}_{n-1}(t) + \boldsymbol{\Lambda}\mathbf{X}_n(t) = \tilde{\mathbf{Y}}_{n-1}(t) + \boldsymbol{\Lambda}\tilde{\mathbf{E}}_n(t), \quad t \in \mathcal{T}, n = 1, 2, \dots, \quad (7)$$

where $\tilde{\mathbf{E}}_n(t) = (\tilde{E}_{n1}(t), \dots, \tilde{E}_{np}(t))^T = \mathbf{X}_n(t) - \tilde{\mathbf{Y}}_{n-1}(t)$, \mathbf{I} is the $p \times p$ identity matrix and $\boldsymbol{\Lambda} = \text{diag}(\lambda_1, \lambda_2, \dots, \lambda_p)$, with $\lambda_j \in (0, 1]$, $j = 1, \dots, p$, the weighting parameters. For $n = 1$, $\tilde{\mathbf{Y}}_0$ represents the starting value, often set equal to the target value $\boldsymbol{\mu}_0$.

By elaborating on Equation (7), we propose the AMFEWMA statistic $\mathbf{Y}_n = (Y_{n1}, \dots, Y_{np})^T$,

defined as follows

$$\mathbf{Y}_n(t) = (\mathbf{I} - \mathbf{\Lambda}_n(t))\mathbf{Y}_{n-1}(t) + \mathbf{\Lambda}_n(t)\mathbf{X}_n(t) = \mathbf{Y}_{n-1}(t) + \mathbf{\Lambda}_n(t)\mathbf{E}_n(t), \quad t \in \mathcal{T}, n = 1, 2, \dots \quad (8)$$

Similarly to $\tilde{\mathbf{E}}_n(t)$, $\mathbf{E}_n(t) = (E_{n1}(t), \dots, E_{np}(t))^T = \mathbf{X}_n(t) - \mathbf{Y}_{n-1}(t)$; while, differently from $\mathbf{\Lambda}$, $\mathbf{\Lambda}_n(t) = \text{diag}(w(E_{n1}(t)), \dots, w(E_{np}(t)))$, where $w(E_{nj}(t)) = \eta(E_{nj}(t))/E_{nj}(t)$ and $\eta(E_{nj}(t))$ is a score function evaluated at the error $E_{nj}(t)$, $j = 1, \dots, p$. In this way, the AMFEWMA statistic \mathbf{Y}_n results in a weighted average of the current observation \mathbf{X}_n and the charting statistic value at the previous time point \mathbf{Y}_{n-1} , as in a conventional EWMA chart, but with weights $w(E_{nj}(t))$ changing over time. That is, the score functions η to be used in Equation (8) are proposed by extending the score functions for a univariate scalar quality characteristic, proposed by Capizzi and Masarotto (2003), to the multivariate functional data setting. A score function $\eta(\cdot)$ must be strictly increasing, odd ($\eta(x) = \eta(-x)$), and such that $\eta(E_{nj}(t))$ is close to $\lambda E_{nj}(t)$ (resp. to $E_{nj}(t)$) when $|E_{nj}(t)|$ is small (resp. is large). Based on these properties, we propose to use as the score function either

$$\eta_1(E_{nj}(t)) = \begin{cases} E_{nj}(t) + (1 - \lambda)C_j(t) & \text{if } E_{nj}(t) < -C_j(t) \\ \lambda E_{nj}(t) & \text{if } |E_{nj}(t)| \leq C_j(t) \\ E_{nj}(t) - (1 - \lambda)C_j(t) & \text{if } E_{nj}(t) > C_j(t) \end{cases}, \quad t \in \mathcal{T}, \quad (9)$$

or

$$\eta_2(E_{nj}(t)) = \begin{cases} E_{nj}(t)[1 - (1 - \lambda)(1 - (E_{nj}(t)/C_j(t))^2)^2] & \text{if } |E_{nj}(t)| \leq C_j(t) \\ E_{nj}(t) & \text{otherwise} \end{cases}, \quad t \in \mathcal{T}, \quad (10)$$

where $\lambda \in (0, 1]$ and $C_j(t) = k\sigma_j(t)$, with k denoting a real positive constant and $\boldsymbol{\sigma} = (\sigma_1, \dots, \sigma_p)^T$ representing the standard deviation function of the current observation \mathbf{X}_n . From Equation (8), it is worth noting that, when \mathbf{X}_n approaches \mathbf{Y}_{n-1} , i.e., $E_{nj}(t)$ tends

to zero through a given score function, the AMFEWMA chart is expected to perform like the MFEWMA control chart based on the statistic $\tilde{\mathbf{Y}}_n$ defined in Equation (7). Instead, it is expected to behave as a Shewhart control chart when $|E_{nj}(t)|$ is large. Hence, the calculation of the AMFEWMA statistic requires the careful selection of the parameters λ and k , which will be addressed in Section 2.4. The functional extension of the classical Hotelling's statistic, based on the AMFEWMA statistic can be defined as

$$V_n^2 = \sum_{i=1}^p \sum_{j=1}^p \int_{\mathcal{T}} \int_{\mathcal{T}} Y_{ni}(s) K_{ij}^*(s, t) Y_{nj}(t) ds dt, \quad (11)$$

where the function K_{ij}^* is defined as

$$K_{ij}^*(s, t) = \sum_{l=1}^L \frac{1}{\rho_l} \psi_{li}(s) \psi_{lj}(t), \quad s, t \in \mathcal{T}, i, j = 1, \dots, p, \quad (12)$$

and $\boldsymbol{\psi}_l = (\psi_{l1}, \dots, \psi_{lp})^T$ denotes the eigenfunctions corresponding to the eigenvalues ρ_l of the asymptotic covariance $\mathbf{C}(s, t)$ of \mathbf{Y}_n , calculated by applying the MFPCA presented in Section 2.2. The number of principal components L is usually chosen such that the retained principal components explain a given fraction of the total variability.

2.4 Design and implementation

The AMFEWMA control chart will be designed to signal when the statistic V_n^2 given in Equation (11) exceeds the upper control limit h chosen as the smallest value achieving an IC ARL larger than or equal to a pre-specified value, usually denoted by ARL_0 . However, to calculate the control limit h , we need to design the AMFEWMA statistics through the selection of the parameters $\boldsymbol{\theta} = (\lambda, k)^T$ involved in the score functions suggested in Equation (9) and Equation (10). In this paper, the optimal parameters are obtained by elaborating on the idea of Capizzi and Masarotto (2003) to provide, to the best possible extent, the AMFEWMA control chart with good performance at different shift magnitudes.

First, a desired ARL_0 , together with two shift values, say $\boldsymbol{\delta}_1$ and $\boldsymbol{\delta}_2$, with $\|\boldsymbol{\delta}_1\| \ll \|\boldsymbol{\delta}_2\|$, and a small positive constant ε (e.g., $\varepsilon = 0.05$) must be chosen. In general $\boldsymbol{\delta}_1$ and $\boldsymbol{\delta}_2$ can represent any “small” and “large” split, respectively, as in Capizzi and Masarotto (2003).

Then, the optimal parameters $\boldsymbol{\theta}$, denoted by $\boldsymbol{\theta}^*$, are found as the solutions of the following problem

$$\boldsymbol{\theta}_2 = \underset{\boldsymbol{\theta}}{\operatorname{argmin}} ARL(\boldsymbol{\delta}_2, \boldsymbol{\theta}) \quad \text{s. t.} \quad ARL(0, \boldsymbol{\theta}) = ARL_0, \quad (13)$$

$$\boldsymbol{\theta}^* = \underset{\boldsymbol{\theta}}{\operatorname{argmin}} ARL(\boldsymbol{\delta}_1, \boldsymbol{\theta}) \quad \text{s. t.} \quad ARL(0, \boldsymbol{\theta}) = ARL_0 \quad \text{and} \quad ARL(\boldsymbol{\delta}_2, \boldsymbol{\theta}) \leq (1 + \varepsilon)ARL(\boldsymbol{\delta}_2, \boldsymbol{\theta}_2), \quad (14)$$

where $ARL(\boldsymbol{\delta}, \boldsymbol{\theta})$ denotes the ARL achieved by the AMFEWMA control chart with parameters $\boldsymbol{\theta}$ when the mean shift is equal to $\boldsymbol{\delta}$. The constant ε allows the AMFEWMA scheme to achieve an ARL at $\boldsymbol{\delta}_2$ that is close to the minimum $ARL(\boldsymbol{\delta}_2, \boldsymbol{\theta}_2)$ while searching for the minimum $ARL(\boldsymbol{\delta}_1, \boldsymbol{\theta})$ with respect to $\boldsymbol{\theta}$. Hereinafter, we will denote the AMFEWMA control chart with parameters $\boldsymbol{\theta}^*$ chosen with the above procedure as AMFEWMA*. It is worth highlighting that the parameters included in the vector $\boldsymbol{\theta}$, and thus $\boldsymbol{\theta}^*$, may vary with respect to the score function used.

To calculate the control limit h , n_{seq} sequences of n_{obs} observations are generated through a bootstrap procedure as proposed by Gandy and Kvaløy (2013) from the Phase I sample. On each sequence, the AMFEWMA statistic and the function K_{ij}^* are calculated as defined in Equation (8) and Equation (12). Then, the monitoring statistic V_n^2 is calculated as defined in Equation (11), respectively. For each sequence, the number of observations acquired up to the first signal of an OC state is stored as a run length (RL), then the ARL is calculated as the average of the RL values over the n_{seq} sequences. The control limit h is then chosen to reach a pre-specified ARL_0 .

Overfitting issues may arise when calculating h (Kruger and Xie, 2012) because the asymptotic covariance of the AMFEWMA statistic \mathbf{Y}_n , used in Equation (11) to calculate V_n^2 , depends on \mathbf{Y}_n itself. Thus, to mitigate this problem, the control limit h will be customarily based on a random subset of the Phase I sample, referred to as the *tuning* set, which is separate from the remaining one used to estimate the covariance of \mathbf{Y}_n , referred to as the *training* set.

In the Phase II monitoring, given the current sequence \mathbf{X}_n , the AMFEWMA statistic \mathbf{Y}_n and the corresponding monitoring statistic V_n^2 are obtained from Equation (8) and Equation

(11), respectively, according to the asymptotic covariance function $\mathbf{C}(s, t)$ estimated in Phase I. An alarm signal is issued if V_n^2 exceeds the control limit h calculated in Phase I. A similar procedure is used in Phase II, where n_{seq}^{II} bootstrap sequences are generated from the Phase II data set, and the ARL is obtained as the average of the RL values calculated for each sequence.

3 Simulation study

The performance of the proposed AMFEWMA control chart in identifying mean shifts in multivariate functional data is evaluated by means of an extensive Monte Carlo simulation study. The data generation process, which is detailed in Supplementary Material A, is performed as in Capezza et al. (2022b) and is inspired by the typical functional form of DRCs in a RSW process, as that introduced in Section 1 and studied in Section 4. Without loss of generality, multivariate functional quality data are generated with $p = 5$ components. Two OC scenarios are considered where the OC observations simulate typical outlying DRCs, based on the work of Xia et al. (2019). In Scenario 1, OC observations mimic a splash weld, which is also known as the expulsion phenomenon and is caused by an excessive welding current flowing through the electrodes. In Scenario 2, they mimic a phase shift of the peak time caused by an overlay large electrode force. In each scenario, six increasing severity levels $SL \in \{0, 1, 2, 3, 4, 5, 6\}$ are explored, where $SL = 0$ means that the process is IC. The severity level quantifies the extent to which Phase II data set profiles deviate from their Phase I counterparts. A higher severity level indicates a greater departure from the baseline and, consequently, a more pronounced OC state for the process. Supplementary Material A defines the severity levels, which can be visually interpreted in Figure A.1 and A.3 that superimpose, on some IC observations, the shifted mean under each shift type, for severity levels $SL \in \{1, 6\}$.

The proposed chart is compared with two competing approaches: the EWMA control chart for multivariate functional data, which is referred to as MFEWMA and based on the Phase II monitoring scheme of Ren et al. (2019) with weighting parameter $\lambda \in \{0.1, 0.2, 0.3, 0.5\}$; and the classical multivariate Shewhart control chart based on the Hotelling T^2 statistic applied to the coefficients obtained from the MFPCA (Capezza et al.,

2023), referred to as SHEWHART.

For each scenario and SL , 30 simulation runs are performed. Each run considers a Phase I sample composed of 2500 observations, with training and tuning samples of 1000 and 1500 observations, respectively. The Phase II data set is composed of 200 sequences of i.i.d. observations with shift locations equal to 100. The AMFEWMA control chart is implemented as detailed in Section 2 with n_{seq} and n_{obs} set equal to 500 and 300, respectively. The parameter L of Equation (12) is chosen such that the retained principal components explain 90% of the total variability.

The AMFEWMA and the competing methods' performance is reported in Table 1 and Table 2 in terms of the estimated ARL , denoted by \widehat{ARL} , as a function of SL for Scenario 1 and Scenario 2, respectively. When the process is IC, the \widehat{ARL} should be as close as possible to ARL_0 , which is set equal to 20, while it should be as small as possible when the process is OC. The AMFEWMA control chart is implemented for $\lambda \in \{0.1, 0.2, 0.3, 0.5\}$ and score function $\eta_1(\cdot)$ as reported in Equation (9) with $k \in \{2, 3, 4\}$, whereas the AMFEWMA* is obtained with optimal parameters θ^* chosen through the algorithm presented in Section 2.4. In the latter, the values of δ_1 and δ_2 are set as $\delta_1 = \hat{\mu}_0 + 0.5\hat{\sigma}$ and $\delta_2 = \hat{\mu}_0 + 2\hat{\sigma}$, where the sample mean $\hat{\mu}_0$ and standard deviation $\hat{\sigma}$ functions are estimated based on 100 bootstrap samples drawn from the Phase I sample.

In agreement with the literature, Table 1 and Table 2 reveal that, among the competing approaches, the SHEWHART control chart achieves the best performance for large SLs , whereas the MFEWMA with small λ values turn out to be the best approach for small SLs . From these tables, it is clear that the parameters λ and k have a marked impact on the performance of the AMFEWMA control chart in both scenarios. As an example, for $\lambda = 0.2$ and $k = 2$, the proposed control chart, while being optimal for large shifts, achieves unsatisfactory \widehat{ARL} for small shifts, performing very similarly to SHEWART. On the other hand, keeping fixed $\lambda = 0.2$ but setting $k = 4$, the AMFEWMA performs similarly to the MFEWMA. In all cases, for each SL , there is a combination of parameters, e.g., $\lambda = 0.3$ and $k = 3$, for which the AMFEWMA performance is the best approach, or is very close to it. Therefore, the problem of finding optimal parameters θ^* remains indispensable. The \widehat{ARL} s values achieved by the proposed control chart with optimal parameters θ^* , obtained

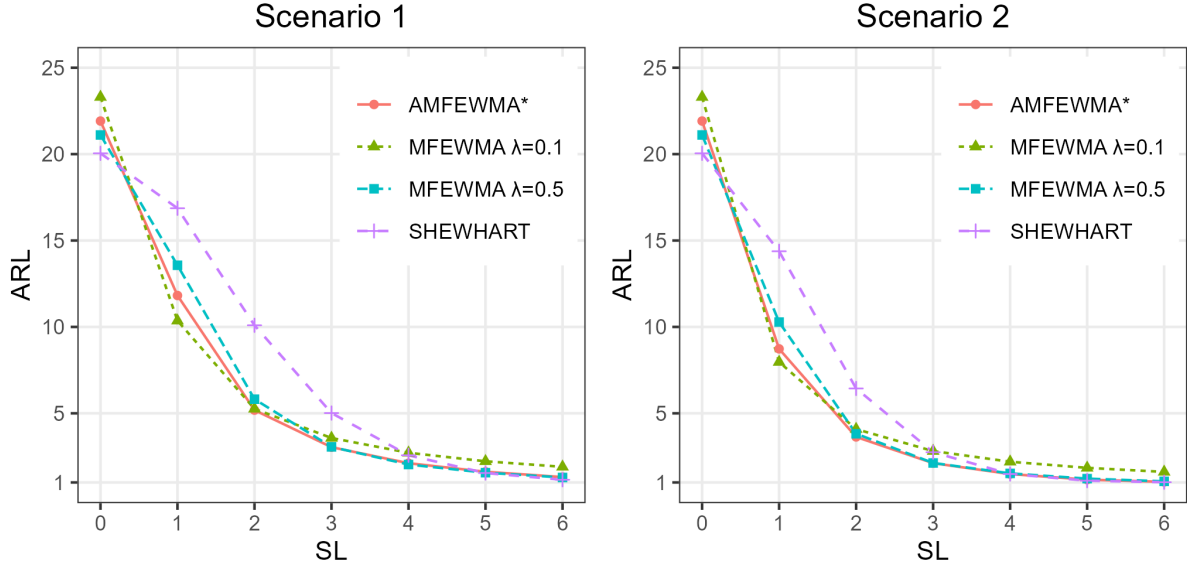


Figure 1: The estimated ARL values for the SHEWHART, MFEWMA (with $\lambda \in \{0.1, 0.5\}$) and the AMFEWMA* control charts in Scenario 1 and Scenario 2.

through the score function η_1 in Equation (9) and referred to as AMFEWMA*, are reported in the last columns of Table 1 and Table 2 and indicate adequate performance for every OC condition considered. Indeed, the AMFEWMA* performs similarly to the MFEWMA control chart with small λ for small SL s, and comparably to the SHEWHART control chart for large SL s. This behavior is graphically shown in Figure 1, which reports the estimated \widehat{ARL} values for the SHEWHART, MFEWMA (with $\lambda \in \{0.1, 0.5\}$) and the AMFEWMA* control charts in Scenario 1 and Scenario 2. From these figures, the \widehat{ARL} s for the AMFEWMA* control chart appears always close to the smallest estimated ARL value, for each SL and scenario considered.

These results are further demonstrated by means of the relative mean index (RMI) suggested by Zou et al. (2012) and defined as

$$RMI = \frac{1}{6} \sum_{SL=1}^6 \frac{ARL_{SL} - sARL_{SL}}{sARL_{SL}},$$

where, at given SL , ARL_{SL} denotes the estimated ARL value of the considered control chart and $sARL_{SL}$ the smallest estimated ARL value among the competitors. The ratio $\frac{ARL_{SL} - sARL_{SL}}{sARL_{SL}}$ can be regarded as a relative efficiency measure of the considered control

chart with respect to the best competitor, at given a SL , while the RMI represents its average over different SL s. The smaller the RMI , the better the overall performance of the control chart. Table 3 shows the RMI achieved by the SHEWHART, the MFEWMA (with $\lambda \in \{0.1, 0.2, 0.3, 0.5\}$), and the AMFEWMA* control charts in Scenario 1 and Scenario 2. In both scenarios, the AMFEWMA* confirms to outperform the competing methods also in terms of RMI . It is worth noting that the SHEWHART control chart and MFEWMA scheme with $\lambda = 0.1$, which represent practitioner's standard choices, show very poor performance in both Scenario 1 and Scenario 2 and thus they should be used with care unless the size of the potential OC condition is known a priori.

Table 1: The estimated ARL values as a function of the severity level SL for Scenario 1. The AMFEWMA control chart is implemented with $\lambda \in \{0.1, 0.2, 0.3, 0.5\}$ and $k \in \{2, 3, 4\}$. The smallest \widehat{ARL} in each row is highlighted in bold when $SL \neq 0$.

SL	SHEWHART	MFEWMA				AMFEWMA ($k = 2$)				AMFEWMA ($k = 3$)				AMFEWMA ($k = 4$)				AMFEWMA*
		λ				λ				λ				λ				
		0.1	0.2	0.3	0.5	0.1	0.2	0.3	0.5	0.1	0.2	0.3	0.5	0.1	0.2	0.3	0.5	
0	20.05	23.30	21.95	21.92	21.11	21.09	21.10	20.84	20.98	22.50	21.54	21.63	21.08	23.38	21.90	21.67	21.02	21.92
1	14.38	7.97	8.04	8.67	10.28	10.87	10.60	10.75	11.81	8.36	8.29	8.92	10.68	8.00	8.09	8.69	10.35	8.73
2	6.44	4.09	3.71	3.62	3.82	4.08	3.86	3.84	4.23	3.81	3.60	3.57	3.84	4.03	3.69	3.60	3.83	3.63
3	2.75	2.82	2.44	2.27	2.13	1.97	1.93	1.93	2.01	2.21	2.14	2.07	2.05	2.71	2.39	2.23	2.11	2.12
4	1.49	2.20	1.88	1.72	1.52	1.29	1.27	1.27	1.30	1.45	1.47	1.45	1.39	1.98	1.78	1.65	1.49	1.49
5	1.10	1.84	1.58	1.42	1.22	1.06	1.05	1.06	1.06	1.13	1.15	1.14	1.11	1.50	1.39	1.31	1.18	1.16
6	1.01	1.61	1.36	1.20	1.06	1.01	1.01	1.01	1.01	1.02	1.03	1.03	1.02	1.19	1.15	1.10	1.04	1.03

Table 2: The estimated ARL values as a function of the severity level SL for Scenario 2. The AMFEWMA control chart is implemented with $\lambda \in \{0.1, 0.2, 0.3, 0.5\}$ and $k \in \{2, 3, 4\}$. The smallest \widehat{ARL} in each row is highlighted in bold when $SL \neq 0$.

SL	SHEWHART	MFEWMA				AMFEWMA ($k = 2$)				AMFEWMA ($k = 3$)				AMFEWMA ($k = 4$)				AMFEWMA*
		λ				λ				λ				λ				
		0.1	0.2	0.3	0.5	0.1	0.2	0.3	0.5	0.1	0.2	0.3	0.5	0.1	0.2	0.3	0.5	
0	20.05	23.30	21.95	21.92	21.11	21.09	21.10	20.84	20.98	22.50	21.54	21.63	21.08	23.38	21.90	21.67	21.02	21.92
1	16.87	10.36	10.75	11.73	13.57	13.69	13.49	13.97	14.77	10.94	11.17	12.17	14.04	10.38	10.88	11.79	13.64	11.82
2	10.09	5.26	5.04	5.09	5.82	6.20	5.95	6.03	6.87	5.24	5.06	5.16	6.03	5.26	5.04	5.10	5.84	5.19
3	5.02	3.57	3.17	3.02	3.06	3.21	3.08	3.07	3.26	3.29	3.07	2.97	3.08	3.53	3.16	3.02	3.07	3.04
4	2.57	2.72	2.36	2.19	2.04	1.96	1.91	1.89	1.93	2.29	2.16	2.06	1.98	2.66	2.34	2.17	2.02	2.11
5	1.54	2.22	1.91	1.75	1.56	1.40	1.39	1.38	1.38	1.68	1.63	1.57	1.48	2.13	1.86	1.72	1.55	1.62
6	1.16	1.90	1.63	1.49	1.29	1.13	1.13	1.13	1.13	1.33	1.31	1.28	1.20	1.75	1.56	1.44	1.27	1.31

Table 3: The RMI for the SHEWHART, MFEWMA (with $\lambda \in \{0.1, 0.2, 0.3, 0.5\}$), and the AMFEWMA* control charts in Scenario 1 and Scenario 2.

	SHEWHART	MFEWMA				AMFEWMA*
		λ				
		0.1	0.2	0.3	0.5	
Scenario 1	1.88	2.36	1.32	0.88	0.59	0.27
Scenario 2	2.55	1.81	0.99	0.73	0.66	0.49

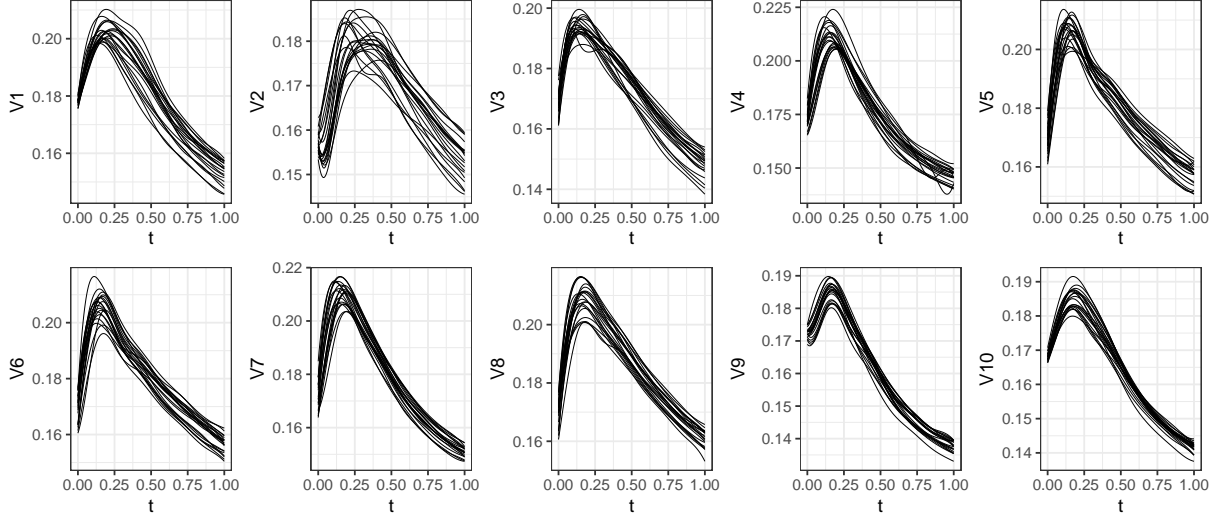


Figure 2: A sketch of DRCs pertaining to the ten spot welds measured on 20 car bodies randomly selected from the dataset analyzed in the case study.

4 Case study

The case study on the SPM of an RSW process in automotive body-in-white manufacturing, mentioned in the introduction, is presented to demonstrate the practical applicability of the proposed AMFEWMA control chart as well as to confirm its superior performance over competitors. Data analyzed are courtesy of Centro Ricerche Fiat and are recorded at the Mirafiori Factory during lab tests on different bodies of the same car model. Each body is characterized by the same large number of spot welds and different characteristics, e.g., metal sheet thickness and material and the welding time.

The case study focuses on a set of $p = 10$ spot welds made by the same welding gun on $n = 1340$ car bodies. That is, for each car body, we consider the multivariate functional quality characteristic represented by the vector of $p = 10$ DRCs relative to the same ten spot welding points. For each DRC, raw measurements were collected at a regular grid of points equally spaced by 1 ms, normalized on the time domain $[0, 1]$. To provide a sketch of the data, the 10-dimensional vectors of DRCs corresponding to 20 random car bodies out of $n = 1340$ are displayed in Figure 2.

Even though this is not meant to be the routine application, to allow for further comparison with competing control charting schemes based on this case study, the Phase I sample has been formed by selecting 568 multivariate profiles observed immediately after

the renewal, which the electrodes are routinely subject to for neutralizing the wear effect that is known, as mentioned in the introduction, to impact on the quality of the final welded point. The remaining 772 observations are grouped into three data sets of 220, 368, and 184 observations, corresponding to three incremental electrode wear levels, namely wear levels 1, 2, and 3, respectively. These three data sets are then used as Phase II observations to evaluate the proposed chart performance with respect to different levels of shift connected with wear level. It is important to emphasize that this is a special case where information regarding electrode wear is available because the data are acquired during lab tests, while such information is commonly out of reach. Hence, a control chart capable of accommodating varying degrees of mean shift, contingent upon different levels of wear, without prior knowledge of the wear levels, can prove immensely advantageous.

The AMFEWMA control chart is implemented as in Section 3 and the 568 observations of the Phase I sample are randomly split into a training and a tuning set, with equal sample sizes. The optimal parameters $\lambda^* = 0.5$ and $k^* = 4$ used in the AMFEWMA* are obtained from Equation (14) through the score function η_1 reported in Equation (9). The bootstrap method presented in Section 2.4 is applied to each of the three Phase II data sets to generate 200 sequences of 200 observations.

Figure 3 shows the AMFEWMA* application to the Phase II monitoring of the three Phase II data sets corresponding to three increasing wear levels. In each plot, the first 100 observations are randomly sampled from the tuning set, whereas the Phase II observations for each wear level considered are displayed on the right of the dashed vertical line. From this figure, the AMFEWMA* scheme clearly appears to adequately detect the mean shift under all shift severity levels. The AMFEWMA performance is further compared in this case study with the competing methods, in terms of ARL, and the results are shown in Table 4. For wear level 1, the MFEWMA control chart with $\lambda = 0.5$ achieves the lowest ARL value, whereas in the other cases, the SHEWHART control chart achieves the best performance. It is easy to note that, as expected, the performance of the AMFEWMA chart is always very close to the best-performing competitor. Therefore, it can be regarded as the best overall choice in all cases where there is no prior information about the severity of the OC scenario.

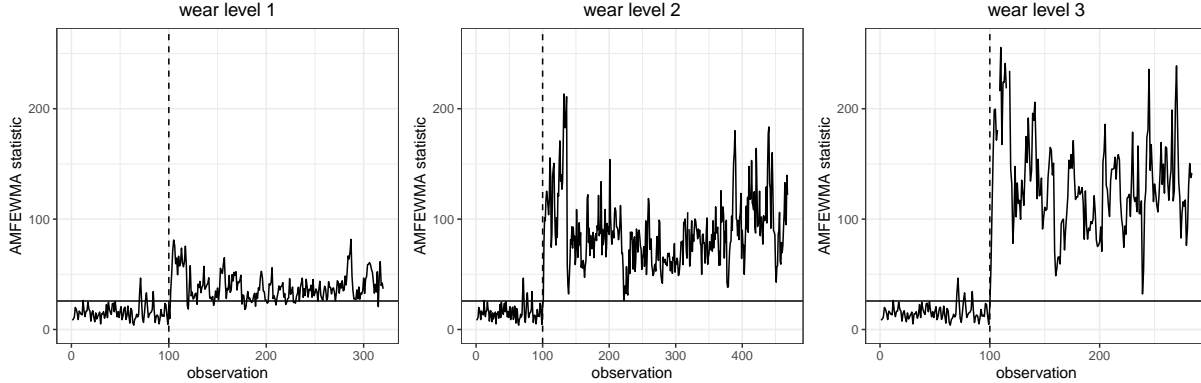


Figure 3: AMFEWMA* control chart under wear levels 1, 2, and 3. In each plot, the first 100 observations are randomly sampled from the tuning set, while the Phase II observations are reported after the dashed vertical line.

Table 4: ARL calculated on the three Phase II data sets (corresponding to wear level 1, 2, and 3, respectively) in the case study, for the proposed AMFEWMA and the competing control charts. In bold, the lowest ARL value for each row is reported.

Wear level	SHEWHART	MFEWMA				AMFEWMA* $\lambda = 0.5, k = 4$
		$\lambda=0.1$	$\lambda=0.2$	$\lambda=0.3$	$\lambda=0.5$	
1	5.68	3.69	3.095	2.91	2.905	2.92
2	1.25	2.185	1.715	1.52	1.315	1.3
3	1.025	1.695	1.415	1.295	1.12	1.085

5 Conclusions

A new control chart for the statistical process control of multivariate functional data is proposed and referred to as adaptive multivariate functional exponentially weighted moving average (EWMA) control chart (AMFEWMA). The AMFEWMA chart is the first EWMA scheme that is able to adaptively monitor a multivariate functional quality characteristic. Whereas, methods already presented in the literature either apply the conventional EWMA approach to multivariate or univariate functional data. Through an extensive Monte Carlo simulation, the performance of the AMFEWMA chart is compared with two competing methods, which proved the AMFEWMA to outperform competing methods in the correct identification of out-of-control (OC) scenarios when the magnitude of the mean shift is unknown. For small shifts, the AMFEWMA performs as the conventional MFEWMA control chart, whereas, for large shifts, it performs as the Shewart control chart. The ability of the proposed method to deal with multivariate functional data and effectively signal process mean shifts in a wide range of severity levels is of paramount importance to protect modern industrial processes where many functional quality characteristics are

routinely available in line against OC scenarios with different severity levels.

Supplementary Materials

The Supplementary Materials contain additional details about the data generation process in the simulation study as well as the R code to reproduce graphs and results over competing methods.

Data Availability Statement

The authors confirm that the data supporting the findings of this study are available within the article and its supplementary materials.

Acknowledgements

The authors are extremely grateful to CRFWCM R&I (World Class Manufacturing Research and Innovation) sites of Orbassano and CampusMelfi, for the access to experimental data and the technological insights in the interpretation of the results.

Funding

The contribution of A. Lepore and F. Centofanti has been economically supported by Piano Nazionale di Ripresa e Resilienza (PNRR) - Missione 5 Componente 2, Investimento 1.3-D.D. 1551.11-10-2022, PE00000004 within the Extended Partnership MICS (Made in Italy - Circular and Sustainable). The activity of B. Palumbo is supported by the MOST - Sustainable Mobility National Research Center and received funding from the European Union Next-GenerationEU (PIANO NAZIONALE DI RIPRESA E RESILIENZA (PNRR) - MISSIONE 4 COMPONENTE 2, INVESTIMENTO 1.4 - D.D. 1033 17/06/2022, CN00000023). This manuscript reflects only the authors' views and opinions, neither the European Union nor the European Commission can be considered responsible for them.

References

- Capezza, C., Centofanti, F., Lepore, A., Menafoglio, A., Palumbo, B., and Vantini, S. (2022a). Functional regression control chart for monitoring ship CO₂ emissions. *Quality and Reliability Engineering International*, 38(3):1519–1537.
- Capezza, C., Centofanti, F., Lepore, A., Menafoglio, A., Palumbo, B., and Vantini, S. (2023). funcharts: Control charts for multivariate functional data in R. *Journal of Quality Technology*.
- Capezza, C., Centofanti, F., Lepore, A., and Palumbo, B. (2021). Functional clustering methods for resistance spot welding process data in the automotive industry. *Applied Stochastic Models in Business and Industry*, 37(5):908–925.
- Capezza, C., Centofanti, F., Lepore, A., and Palumbo, B. (2022b). Robust multivariate functional control charts. *arXiv preprint arXiv:2207.07978*.
- Capezza, C., Lepore, A., Menafoglio, A., Palumbo, B., and Vantini, S. (2020). Control charts for monitoring ship operating conditions and CO₂ emissions based on scalar-on-function regression. *Applied Stochastic Models in Business and Industry*, 36(3):477–500.
- Capizzi, G. and Masarotto, G. (2003). An adaptive exponentially weighted moving average control chart. *Technometrics*, 45(3):199–207.
- Cardot, H., Ferraty, F., and Sarda, P. (2003). Spline estimators for the functional linear model. *Statistica Sinica*, pages 571–591.
- Centofanti, F., Lepore, A., Kulahci, M., and Spooner, M. P. (2022). Real-time monitoring of functional data. *arXiv preprint arXiv:2205.06256*.
- Centofanti, F., Lepore, A., Menafoglio, A., Palumbo, B., and Vantini, S. (2021). Functional regression control chart. *Technometrics*, 63(3):281–294.
- Chan, L. K. and Zhang, J. (2000). Some issues in the design of EWMA charts. *Communications in Statistics-Simulation and Computation*, 29(1):201–217.
- Chiou, J.-M., Chen, Y.-T., and Yang, Y.-F. (2014). Multivariate functional principal component analysis: A normalization approach. *Statistica Sinica*, pages 1571–1596.
- Chou, S.-H., Chang, S. I., and Tsai, T.-R. (2014). On monitoring of multiple non-linear profiles. *International Journal of Production Research*, 52(11):3209–3224.

- Colosimo, B. M. and Pacella, M. (2010). A comparison study of control charts for statistical monitoring of functional data. *International Journal of Production Research*, 48(6):1575–1601.
- Crowder, S. V. (1989). Design of exponentially weighted moving average schemes. *Journal of Quality technology*, 21(3):155–162.
- De Boor, C. (1978). *A practical guide to splines*, volume 27. springer-verlag New York.
- Fassò, A., Toccu, M., and Magno, M. (2016). Functional control charts and health monitoring of steam sterilizers. *Quality and Reliability Engineering International*, 32(6):2081–2091.
- Gan, F. (1993). An optimal design of EWMA control charts based on median run length. *Journal of Statistical Computation and Simulation*, 45(3-4):169–184.
- Gandy, A. and Kvaløy, J. T. (2013). Guaranteed conditional performance of control charts via bootstrap methods. *Scandinavian Journal of Statistics*, 40(4):647–668.
- Grasso, M., Colosimo, B. M., and Pacella, M. (2014). Profile monitoring via sensor fusion: the use of PCA methods for multi-channel data. *International Journal of Production Research*, 52(20):6110–6135.
- Grasso, M., Colosimo, B. M., and Tsung, F. (2017). A phase I multi-modelling approach for profile monitoring of signal data. *International Journal of Production Research*, 55(15):4354–4377.
- Grasso, M., Menafoglio, A., Colosimo, B. M., and Secchi, P. (2016). Using curve-registration information for profile monitoring. *Journal of Quality Technology*, 48(2):99–127.
- Green, P. J. and Silverman, B. W. (1993). *Nonparametric regression and generalized linear models: a roughness penalty approach*. Crc Press.
- Happ, C. and Greven, S. (2018). Multivariate functional principal component analysis for data observed on different (dimensional) domains. *Journal of the American Statistical Association*, 113(522):649–659.
- Haq, A. and Khoo, M. B. (2019). An adaptive multivariate ewma chart. *Computers & Industrial Engineering*, 127:549–557.
- Jin, J. and Shi, J. (1999). Feature-preserving data compression of stamping tonnage information using wavelets. *Technometrics*, 41(4):327–339.
- Jolliffe, I. T. and Cadima, J. (2016). Principal component analysis: a review and recent de-

- velopments. *Philosophical Transactions of the Royal Society A: Mathematical, Physical and Engineering Sciences*, 374(2065):20150202.
- Jones, C. L., Abdel-Salam, A.-S. G., and Mays, D. (2021). Practitioners guide on parametric, nonparametric, and semiparametric profile monitoring. *Quality and Reliability Engineering International*, 37(3):857–881.
- Jones, L. A., Champ, C. W., and Rigdon, S. E. (2001). The performance of exponentially weighted moving average charts with estimated parameters. *Technometrics*, 43(2):156–167.
- Knoth, S. (2007). Accurate ARL calculation for EWMA control charts monitoring normal mean and variance simultaneously. *Sequential Analysis*, 26(3):251–263.
- Kokoszka, P. and Reimherr, M. (2017). *Introduction to functional data analysis*. Chapman and Hall/CRC.
- Kruger, U. and Xie, L. (2012). *Statistical monitoring of complex multivariate processes: with applications in industrial process control*. John Wiley & Sons.
- Lowry, C. A., Woodall, W. H., Champ, C. W., and Rigdon, S. E. (1992). A multivariate exponentially weighted moving average control chart. *Technometrics*, 34(1):46–53.
- Lucas, J. M. and Saccucci, M. S. (1990). Exponentially weighted moving average control schemes: properties and enhancements. *Technometrics*, 32(1):1–12.
- Mahmoud, M. A. and Zahran, A. R. (2010). A multivariate adaptive exponentially weighted moving average control chart. *Communications in Statistics—Theory and Methods*, 39(4):606–625.
- Maleki, M. R., Amiri, A., and Castagliola, P. (2018). An overview on recent profile monitoring papers (2008–2018) based on conceptual classification scheme. *Computers & Industrial Engineering*, 126:705–728.
- Manladan, S., Yusof, F., Ramesh, S., Fadzil, M., Luo, Z., and Ao, S. (2017). A review on resistance spot welding of aluminum alloys. *The International Journal of Advanced Manufacturing Technology*, 90(1):605–634.
- Martín, Ó., Pereda, M., Santos, J. I., and Galán, J. M. (2014). Assessment of resistance spot welding quality based on ultrasonic testing and tree-based techniques. *Journal of Materials Processing Technology*, 214(11):2478–2487.

- Menafoglio, A., Grasso, M., Secchi, P., and Colosimo, B. M. (2018). Profile monitoring of probability density functions via simplicial functional pca with application to image data. *Technometrics*, 60(4):497–510.
- Montgomery, D. C. (2019). *Introduction to statistical quality control*. John Wiley & Sons.
- Noorossana, R., Saghaei, A., and Amiri, A. (2011). *Statistical analysis of profile monitoring*. John Wiley & Sons.
- Paynabar, K., Zou, C., and Qiu, P. (2016). A change-point approach for phase-I analysis in multivariate profile monitoring and diagnosis. *Technometrics*, 58(2):191–204.
- Qiu, P. (2014). *Introduction to statistical process control*. CRC press.
- R Core Team (2023). *R: A Language and Environment for Statistical Computing*. R Foundation for Statistical Computing, Vienna, Austria.
- Ramsay, J. and Silverman, B. (2005). *Functional data analysis*. Springer.
- Ren, H., Chen, N., and Wang, Z. (2019). Phase-II monitoring in multichannel profile observations. *Journal of Quality Technology*, 51(4):338–352.
- Serel, D. A. (2009). Economic design of EWMA control charts based on loss function. *Mathematical and Computer Modelling*, 49(3-4):745–759.
- Wang, Y., Mei, Y., and Paynabar, K. (2018). Thresholded multivariate principal component analysis for phase I multichannel profile monitoring. *Technometrics*, 60(3):360–372.
- Xia, Y.-J., Su, Z.-W., Li, Y.-B., Zhou, L., and Shen, Y. (2019). Online quantitative evaluation of expulsion in resistance spot welding. *Journal of Manufacturing Processes*, 46:34–43.
- Zhang, H. and Senkara, J. (2011). *Resistance welding: fundamentals and applications*. CRC press.
- Zou, C., Ning, X., and Tsung, F. (2012). Lasso-based multivariate linear profile monitoring. *Annals of operations research*, 192(1):3–19.

Supplementary Materials to “An Adaptive Multivariate Functional EWMA Control Chart”

A Details on Data Generation in the Simulation Study

The data generation process is inspired by the real-case study in Section 4 and mimics typical behaviors of DRCs in an RSW process. The data correlation structure is generated similarly to Centofanti et al. (2021); Capezza et al. (2022). The compact domain \mathcal{T} is set, without loss of generality, equal to $[0, 1]$, and the number components p is set equal to 5. The eigenfunction set $\{\psi_i\}$ is generated by considering the correlation function \mathbf{G} through the following steps.

1. Set the diagonal elements G_{ll} , $l = 1, \dots, p$ of \mathbf{G} as the *Bessel* correlation function of the first kind (Abramowitz and Stegun, 1964). The general form of the correlation function and parameter used are listed in Table Then, calculate the eigenvalues $\{\eta_{lk}^X\}$ and the corresponding eigenfunctions $\{\vartheta_{lk}\}$, $k = 1, 2, \dots$, of G_{ll} , $l = 1, \dots, p$.
2. Obtain the cross-correlation function G_{lj} , $l, j = 1, \dots, p$ and $l \neq j$, by

$$G_{lj}(t_1, t_2) = \sum_{k=1}^{\infty} \frac{\eta_k}{1 + |l - j|} \vartheta_{lk}(t_1) \vartheta_{jk}(t_2) \quad t_1, t_2 \in \mathcal{T}. \quad (\text{A.1})$$

3. Calculate the eigenvalues $\{\lambda_i\}$ and the corresponding eigenfunctions $\{\psi_i\}$ through the spectral decomposition of $\mathbf{G} = \{G_{lj}\}_{l,j=1,\dots,p}$, for $i = 1, \dots, L^*$.

Further, L^* is set equal to 10. Let $\mathbf{Z} = (Z_1, \dots, Z_p)$ as

$$\mathbf{Z} = \sum_{i=1}^{L^*} \xi_i \psi_i. \quad (\text{A.2})$$

Table 1. Bessel correlation function and parameter for data generation in the simulation study.

	ρ	ν
$J_\nu(z) = \left(\frac{ z /\rho}{2}\right)^\nu \sum_{j=0}^{\infty} \frac{(-(z /\rho)^2/4)^j}{j!\Gamma(\nu+j+1)}$	0.125	0

with $\boldsymbol{\xi}_{L^*} = (\xi_1^X, \dots, \xi_{L^*}^X)^T$ generated by means of a multivariate normal distribution with covariance $\text{Cov}(\boldsymbol{\xi}_{L^*}^X) = \boldsymbol{\Lambda}^{\mathbf{X}} = \text{diag}(\lambda_1, \dots, \lambda_{L^*})$.

Furthermore, let the mean process m

$$m(t) = 0.2074 + 0.3117 \exp(-371.4t) + 0.5284(1 - \exp(0.8217t)) - 423.3 [1 + \tanh(-26.15(t + 0.1715))] \quad t \in \mathcal{T}. \quad (\text{A.3})$$

Note that the mean function m is generated to resemble a typical DRC through the phenomenological model for the RSW process presented in Schwab et al. (2012). Then, let define the contamination models C_E and C_P , which mimics a splash weld (expulsion) and phase shift of the peak time, as

$$C_E(t) = \min \left\{ 0, -2M_E(t - 0.5) \right\} \quad t \in \mathcal{T}, \quad (\text{A.4})$$

and

$$C_P(t) = -m(t) - (M_P/20)t + 0.2074 + 0.3117 \exp(-371.4h(t)) + 0.5284(1 - \exp(0.8217h(t))) - 423.3 [1 + \tanh(-26.15(h(t) + 0.1715))] \quad t \in \mathcal{T}, \quad (\text{A.5})$$

where $h : \mathcal{T} \rightarrow \mathcal{T}$ transforms the temporal dimension t as follows

$$h(t) = \begin{cases} t & \text{if } t \leq 0.05 \\ \frac{0.55 - M_P}{0.55}t - \left(1 + \frac{0.55 - M_P}{0.55}\right)0.05 & \text{if } 0.05 < t \leq 0.6 \\ \frac{0.4 + M_P}{0.4}t + 1 - \frac{0.4 + M_P}{0.4} & \text{if } t > 0.6, \end{cases} \quad (\text{A.6})$$

Table 2. Parameters used to generate the Phase II sample for Scenario 1 and Scenario 2 and shift level $SL = \{0, 1, 2, 3, 4, 5, 6\}$ in the simulation study.

SL	Scenario 1		Scenario 2	
	$B_E = 1, B_P = 0$		$B_E = 0, B_P = 1$	
	M_E	M_P	M_E	M_P
1	0.0019	0.00	0.00	0.025
2	0.0038	0.00	0.00	0.050
3	0.0056	0.00	0.00	0.075
4	0.0075	0.00	0.00	0.100
5	0.0094	0.00	0.00	0.125
6	0.0112	0.00	0.00	0.150

and M_E and M_P are contamination sizes. Then, the model to generate $\mathbf{X} = (X_1, \dots, X_p)^T$ is

$$\mathbf{X}(t) = \mathbf{m}(t) + \mathbf{Z}(t)\sigma + \boldsymbol{\varepsilon}(t) + B_E \mathbf{C}_E(t) + B_P \mathbf{C}_P(t) \quad t \in \mathcal{T}, \quad (\text{A.7})$$

where \mathbf{m} is a p dimensional vector with components equal to m , $\sigma > 0$, $\boldsymbol{\varepsilon} = (\varepsilon_1, \dots, \varepsilon_p)^T$, where ε_i are white noise functions such that for each $t \in [0, 1]$, $\varepsilon_i(t)$ are normal random variables with zero mean and standard deviation σ_e , $\mathbf{C}_E = (C_E, \dots, C_E)^T$ and $\mathbf{C}_P = (C_P, \dots, C_P)^T$.

Then, the Phase I observations are generated through Equation (A.7) with $B_E = B_P = 0$. The Phase II sample is generated through Equation (A.7) by considering the parameters listed in Table 2 for Scenario 1 and Scenario 2, with $\sigma_e = 0.005$ and $\sigma = 0.002$. In Scenario 1, OC observations mimic a splash weld (expulsion) caused by excessive welding current, while, in Scenario 2, they are generated with a phase shift of the peak time caused by an increased force applied to the electrode used in the welding process (Xia et al., 2019). Finally, the generated data are assumed to be discretely observed at 25 equally spaced time points over the domain $[0, 1]$. For illustrative purposes, a sample of 20 randomly generated realizations of IC observations are shown in Figure A.1. Whereas, Figure A.2 and Figure A.3 show a sample of 100 randomly generated observations in Scenario 1 for models M1, M2, and M3, each type of shift with severity level defined by M_E and M_P in Table 2.

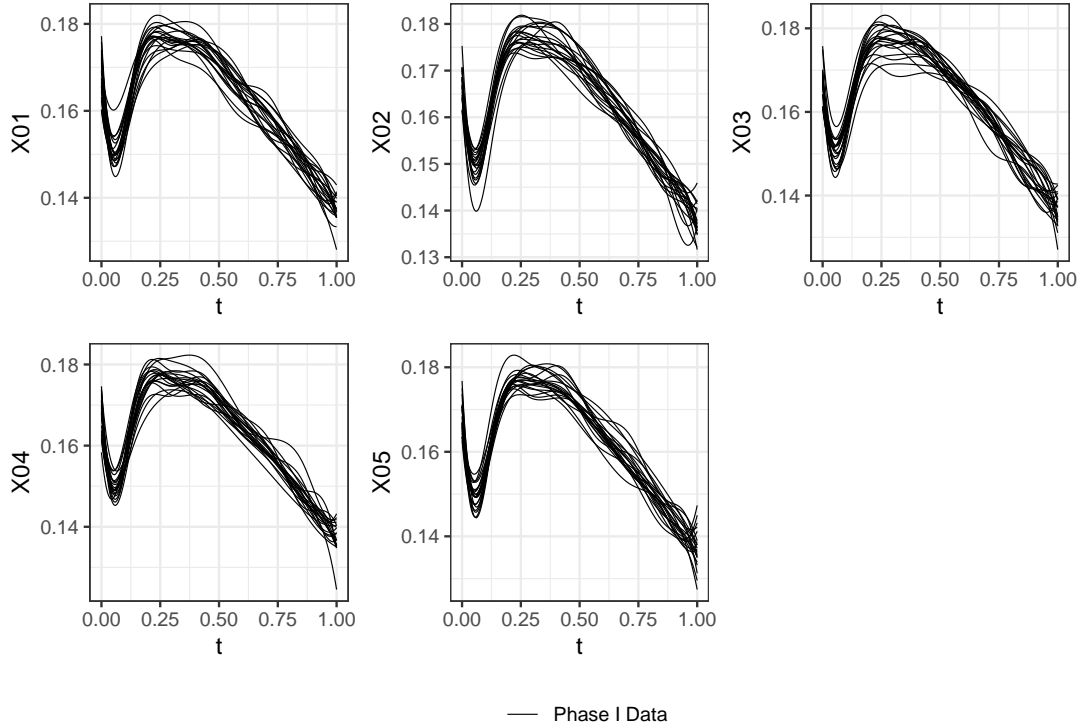


Figure A.1. An example of 20 randomly generated IC observations

References

- Abramowitz, M. and I. A. Stegun (1964). Handbook of mathematical functions: with formulas, graphs, and mathematical tables.
- Capezza, C., F. Centofanti, A. Lepore, and B. Palumbo (2022). Robust multivariate functional control charts. *arXiv preprint arXiv:2207.07978*.
- Centofanti, F., A. Lepore, A. Menafoglio, B. Palumbo, and S. Vantini (2021). Functional regression control chart. *Technometrics* 63(3), 281–294.
- Schwab, I., M. Senn, and N. Link (2012). Improving expert knowledge in dynamic process monitoring by symbolic regression. In *2012 Sixth International Conference on Genetic and Evolutionary Computing*, pp. 132–135. IEEE.
- Xia, Y.-J., Z.-W. Su, Y.-B. Li, L. Zhou, and Y. Shen (2019). Online quantitative evaluation of expulsion in resistance spot welding. *Journal of Manufacturing Processes* 46, 34–43.

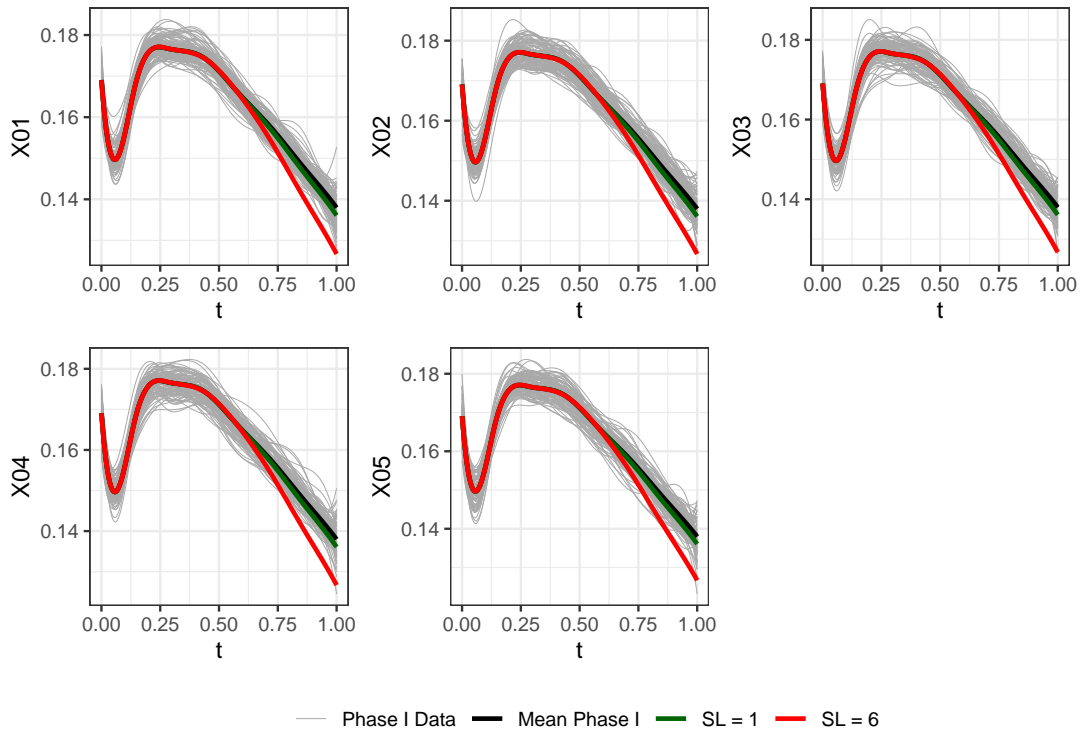


Figure A.2. Simulated data in Scenario 1. Bold lines denote mean functions with $SL = 0$ (Mean Phase I), $SL = 1$ and $SL = 6$.

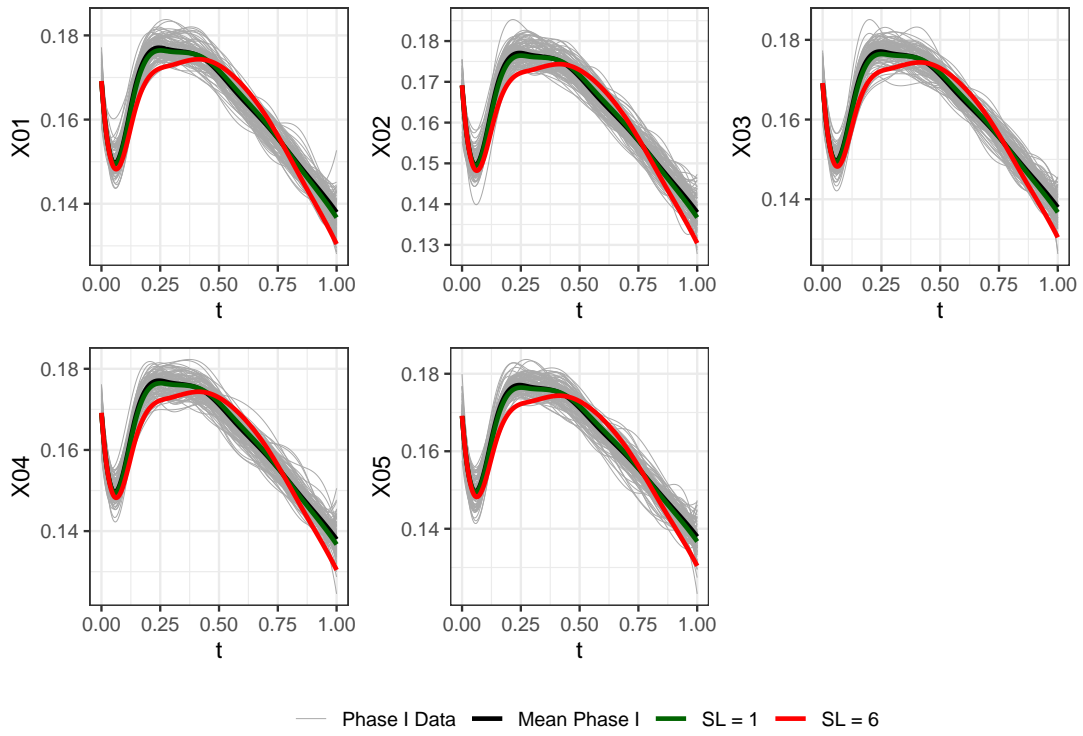


Figure A.3. Simulated data in Scenario 2. Bold lines denote mean functions with $SL = 0$ (Mean Phase I), $SL = 1$ and $SL = 6$.